



<b>Publication Year</b>	2021
<b>Acceptance in OA</b>	2025-03-24T11:37:44Z
<b>Title</b>	Thermally altered subsurface material of asteroid (162173) Ryugu
<b>Authors</b>	Kitazato, K., Milliken, R. E., Iwata, T., Abe, M., Ohtake, M., Matsuura, S., Takagi, Y., Nakamura, T., Hiroi, T., Matsuoka, M., Riu, L., Tsuda, Y., Nakauchi, Y., Tsumura, K., Arai, T., Senshu, H., Hirata, N., Barucci, M. A., Brunetto, R., Pilorget, C., Poulet, F., Bibring, J. -P., Domingue, D. L., Vilas, F., Takir, D., PALOMBA, Ernesto, Galiano, A., PERNA, Davide, Osawa, T., Komatsu, M., Nakato, A., Arai, T., Takato, N., Matsunaga, T., Arakawa, M., Saiki, T., Wada, K., Kadono, T., Imamura, H., Yano, H., Shirai, K., Hayakawa, M., Okamoto, C., Sawada, H., Ogawa, K., Iijima, Y., Sugita, S., Honda, R., Morota, T., Kameda, S., Tatsumi, E., Cho, Y., Yoshioka, K., Yokota, Y., Sakatani, N., Yamada, M., Kouyama, T., Suzuki, H., Honda, C., Namiki, N., Mizuno, T., Matsumoto, K., Noda, H., Ishihara, Y., Yamada, R., Yamamoto, K., Yoshida, F., Abe, S., Higuchi, A., Yamamoto, Y., Okada, T., Shimaki, Y., Noguchi, R., Miura, A., Hirata, N., Tachibana, S., Yabuta, H., Ishiguro, M., Ikeda, H., Takeuchi, H., Shimada, T., Mori, O., Hosoda, S., Tsukizaki, R., Soldini, S., Ozaki, M., Terui, F., Ogawa, N., Mimasu, Y., Ono, G., Yoshikawa, K., Hirose, C., Fujii, A., Takahashi, T., Kikuchi, S., Takei, Y., Yamaguchi, T., Nakazawa, S., Tanaka, S., Yoshikawa, M., Watanabe, S.
<b>Publisher's version (DOI)</b>	10.1038/s41550-020-01271-2
<b>Handle</b>	<a href="http://hdl.handle.net/20.500.12386/36931">http://hdl.handle.net/20.500.12386/36931</a>
<b>Journal</b>	NATURE ASTRONOMY
<b>Volume</b>	5



# Thermally altered subsurface material of asteroid (162173) Ryugu

K. Kitazato<sup>1</sup>✉, R. E. Milliken<sup>2</sup>, T. Iwata<sup>3,4</sup>, M. Abe<sup>3,4</sup>, M. Ohtake<sup>1</sup>, S. Matsuura<sup>5</sup>, Y. Takagi<sup>6</sup>, T. Nakamura<sup>7</sup>, T. Hiroi<sup>2</sup>, M. Matsuoka<sup>3</sup>, L. Riu<sup>3</sup>, Y. Nakauchi<sup>3</sup>, K. Tsumura<sup>8</sup>, T. Arai<sup>9</sup>, H. Senshu<sup>10</sup>, N. Hirata<sup>11</sup>, M. A. Barucci<sup>11</sup>, R. Brunetto<sup>12</sup>, C. Pilorget<sup>12</sup>, F. Poulet<sup>12</sup>, J.-P. Bibring<sup>12</sup>, D. L. Domingue<sup>13</sup>, F. Vilas<sup>13</sup>, D. Takir<sup>14</sup>, E. Palomba<sup>15</sup>, A. Galiano<sup>15</sup>, D. Perna<sup>11,16</sup>, T. Osawa<sup>17</sup>, M. Komatsu<sup>4</sup>, A. Nakato<sup>3</sup>, T. Arai<sup>10</sup>, N. Takato<sup>18</sup>, T. Matsunaga<sup>19</sup>, M. Arakawa<sup>20</sup>, T. Saiki<sup>3</sup>, K. Wada<sup>10</sup>, T. Kadono<sup>21</sup>, H. Imamura<sup>3</sup>, H. Yano<sup>3,4</sup>, K. Shirai<sup>3,20</sup>, M. Hayakawa<sup>3</sup>, C. Okamoto<sup>20,37</sup>, H. Sawada<sup>3</sup>, K. Ogawa<sup>20,22</sup>, Y. Iijima<sup>3,38</sup>, S. Sugita<sup>10,23</sup>, R. Honda<sup>24</sup>, T. Morota<sup>23</sup>, S. Kameda<sup>25</sup>, E. Tatsumi<sup>23,26</sup>, Y. Cho<sup>23</sup>, K. Yoshioka<sup>23</sup>, Y. Yokota<sup>3,24</sup>, N. Sakatani<sup>25</sup>, M. Yamada<sup>10</sup>, T. Kouyama<sup>27</sup>, H. Suzuki<sup>28</sup>, C. Honda<sup>1</sup>, N. Namiki<sup>4,18</sup>, T. Mizuno<sup>3,4</sup>, K. Matsumoto<sup>18</sup>, H. Noda<sup>18</sup>, Y. Ishihara<sup>22</sup>, R. Yamada<sup>1</sup>, K. Yamamoto<sup>18</sup>, F. Yoshida<sup>10,21</sup>, S. Abe<sup>29</sup>, A. Higuchi<sup>21</sup>, Y. Yamamoto<sup>3,4</sup>, T. Okada<sup>3,23</sup>, Y. Shimaki<sup>3</sup>, R. Noguchi<sup>3</sup>, A. Miura<sup>3,4</sup>, N. Hirata<sup>20</sup>, S. Tachibana<sup>3,23</sup>, H. Yabuta<sup>3,30</sup>, M. Ishiguro<sup>31</sup>, H. Ikeda<sup>3</sup>, H. Takeuchi<sup>3,4</sup>, T. Shimada<sup>3</sup>, O. Mori<sup>3</sup>, S. Hosoda<sup>3</sup>, R. Tsukizaki<sup>3</sup>, S. Soldini<sup>32</sup>, M. Ozaki<sup>3,4</sup>, F. Terui<sup>3</sup>, N. Ogawa<sup>3</sup>, Y. Mimasu<sup>3</sup>, G. Ono<sup>33</sup>, K. Yoshikawa<sup>33</sup>, C. Hirose<sup>33</sup>, A. Fujii<sup>3</sup>, T. Takahashi<sup>34</sup>, S. Kikuchi<sup>3</sup>, Y. Takei<sup>3,33</sup>, T. Yamaguchi<sup>35</sup>, S. Nakazawa<sup>3</sup>, S. Tanaka<sup>3,4</sup>, M. Yoshikawa<sup>3,4</sup>, S. Watanabe<sup>3,36</sup> and Y. Tsuda<sup>3,4</sup>

Analyses of meteorites and theoretical models indicate that some carbonaceous near-Earth asteroids may have been thermally altered due to radiative heating during close approaches to the Sun<sup>1–3</sup>. However, the lack of direct measurements on the subsurface doesn't allow us to distinguish it from parent-body processes. In April 2019, the Hayabusa2 mission successfully completed an artificial impact experiment on the carbonaceous near-Earth asteroid (162173) Ryugu<sup>4,5</sup>, which provided an opportunity to investigate exposed subsurface material and test potential effects of radiative heating. Here we report observations of Ryugu's subsurface material by the Near-Infrared Spectrometer (NIRS3) on the Hayabusa2 spacecraft. Reflectance spectra of excavated material exhibit a hydroxyl (OH) absorption feature that is slightly stronger and peak-shifted compared with that observed for the sur-

face, indicating that space weathering and/or radiative heating have caused subtle spectral changes in the uppermost surface. The strength and shape of the OH feature suggests that the subsurface material experienced heating above 300 °C, similar to the surface. In contrast, thermophysical modelling indicates that radiative heating cannot increase the temperature above 200 °C at the estimated excavation depth of 1 m, even at the smallest heliocentric distance possible for Ryugu. This supports the hypothesis that primary thermal alteration occurred on Ryugu's parent body.

On 5 April 2019, the Japan Aerospace Exploration Agency's (JAXA) Hayabusa2 spacecraft carried out an artificial impact experiment on the surface of Ryugu using the Small Carry-on Impactor (SCI)<sup>4,5</sup>. The SCI module was separated from the spacecraft at 0.5 km altitude and fired a 2 kg copper projectile at a velocity of

<sup>1</sup>The University of Aizu, Fukushima, Japan. <sup>2</sup>Brown University, Providence, RI, USA. <sup>3</sup>Institute of Space and Astronautical Science (ISAS), Japan Aerospace Exploration Agency (JAXA), Sagami-hara, Japan. <sup>4</sup>The Graduate University for Advanced Studies (SOKENDAI), Kanagawa, Japan. <sup>5</sup>Kwansei Gakuin University, Hyogo, Japan. <sup>6</sup>Aichi Toho University, Nagoya, Japan. <sup>7</sup>Tohoku University, Sendai, Japan. <sup>8</sup>Tokyo City University, Tokyo, Japan. <sup>9</sup>Ashikaga University, Tochigi, Japan. <sup>10</sup>Chiba Institute of Technology, Chiba, Japan. <sup>11</sup>LESIA, Observatoire de Paris, Université PSL, CNRS, Université de Paris, Sorbonne Université, Meudon, France. <sup>12</sup>Institut d'Astrophysique Spatiale, Université Paris-Sud, Orsay, France. <sup>13</sup>Planetary Science Institute, Tucson, AZ, USA. <sup>14</sup>Astromaterials Research and Exploration Science, NASA Johnson Space Center, Houston, TX, USA. <sup>15</sup>Istituto di Astrofisica e Planetologia Spaziali, Istituto Nazionale di Astrofisica (INAF), Rome, Italy. <sup>16</sup>Osservatorio Astronomico di Roma, INAF, Monte Porzio Catone, Italy. <sup>17</sup>Japan Atomic Energy Agency, Ibaraki, Japan. <sup>18</sup>National Astronomical Observatory of Japan, Tokyo, Japan. <sup>19</sup>National Institute for Environmental Studies, Ibaraki, Japan. <sup>20</sup>Kobe University, Kobe, Japan. <sup>21</sup>University of Occupational and Environmental Health, Kitakyushu, Japan. <sup>22</sup>JAXA Space Exploration Center, JAXA, Sagami-hara, Japan. <sup>23</sup>The University of Tokyo, Tokyo, Japan. <sup>24</sup>Kochi University, Kochi, Japan. <sup>25</sup>Rikkyo University, Tokyo, Japan. <sup>26</sup>Instituto de Astrofísica de Canarias, University of La Laguna, Tenerife, Spain. <sup>27</sup>National Institute of Advanced Industrial Science and Technology, Tokyo, Japan. <sup>28</sup>Meiji University, Tokyo, Japan. <sup>29</sup>Nihon University, Chiba, Japan. <sup>30</sup>Hiroshima University, Hiroshima, Japan. <sup>31</sup>Seoul National University, Seoul, Korea. <sup>32</sup>University of Liverpool, Liverpool, UK. <sup>33</sup>Research and Development Directorate, JAXA, Sagami-hara, Japan. <sup>34</sup>NEC Corporation, Tokyo, Japan. <sup>35</sup>Mitsubishi Electric Corporation, Kanagawa, Japan. <sup>36</sup>Nagoya University, Nagoya, Japan. <sup>37</sup>Deceased: C. Okamoto <sup>38</sup>Deceased: Y. Iijima ✉e-mail: [kitazato@u-aizu.ac.jp](mailto:kitazato@u-aizu.ac.jp)

64 ~2 km s<sup>-1</sup> toward the target site on the equatorial region of Ryugu.  
 65 On 25 April, Hayabusa2 approached the target site and acquired  
 66 images using the Optical Navigation Camera Telescope (ONC-T),  
 67 which showed that a semi-circular shaped crater of 17 m in diameter  
 68 (hereafter referred to as the SCI crater) had been formed at 7.9° N,  
 69 301.3° E (ref. 4). A heterogeneous expansion of ejecta was observed  
 70 by the Deployable Camera (DCAM3) during the SCI experiment,  
 71 and the analysis of the ONC-T images revealed that the excavated  
 72 subsurface material was mainly distributed to the north side of the  
 73 SCI crater<sup>4</sup>. The maximum depth of the SCI crater is ~2.7 m and it  
 74 has been estimated that much of the subsurface material distributed  
 75 on and around the crater would have been ejected from ~1 m  
 76 depth<sup>4</sup>. The SCI experiment thus provides a unique opportunity to  
 77 test the effects of surface modification by radiative heating<sup>1–3</sup> and/  
 78 or space weathering<sup>6</sup>.

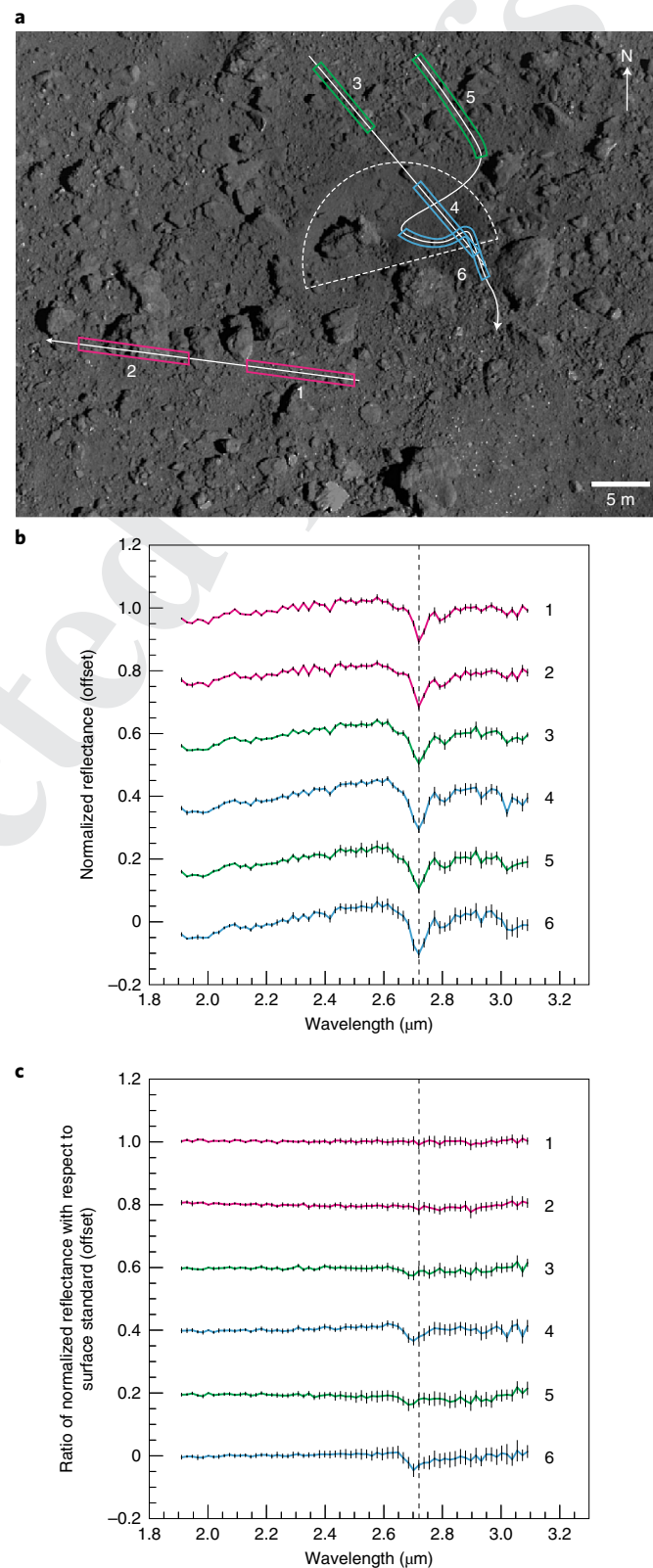
79 Before successfully acquiring a sample from ~20 m to the north-  
 80 east of the SCI crater on 11 July 2019, the Hayabusa2 spacecraft  
 81 performed three descent operations on different days to conduct  
 82 a detailed survey of the impact site. During those descent opera-  
 83 tions, the NIRS3 acquired continuous spectra over a wavelength  
 84 range of 1.8 to 3.2 μm with a 0.1° field of view<sup>7</sup>. Two sites from  
 85 each of the three descent observations were chosen to search for  
 86 spectral differences between typical surface and excavated materi-  
 87 als (see Methods). Figure 1 shows the location of the NIRS3 foot-  
 88 prints and associated reflectance spectra for the six observations of  
 89 the SCI crater region. The NIRS3 footprints of 16 May (sites 1 and  
 90 2) pass through the region south of the crater, whereas those of 30  
 91 May (sites 3 and 4) and 13 June (sites 5 and 6) span the region to  
 92 the north and the crater interior. The distribution of crater ejecta as  
 93 determined from the ONC-T and DCAM3 images reveals that sites  
 94 1 and 2 and sites 3–6 correspond to ejecta-free and ejecta-rich areas,  
 95 respectively<sup>4</sup>. All the spectra, including those over ejecta-rich areas,  
 96 exhibit a weak and narrow OH feature with a reflectance minimum  
 97 at 2.72 μm. This is similar to the spectral feature observed across  
 98 the entire surface of Ryugu<sup>8</sup> and indicates that the subsurface material  
 99 in this region has been thermally altered to the same degree as the  
 100 surface material.

101 Spectral differences between surface and subsurface were fur-  
 102 ther evaluated by comparing the spectra observed for the SCI crater  
 103 region with those from regions far from the impact site. Figure 1c  
 104 shows the ratio of normalized reflectance spectra between the SCI  
 105 crater region and a surface ‘standard’ (a region chosen to represent  
 106 typical spectral properties of Ryugu; see Methods). The ratio spectra  
 107 of sites 1 and 2 are almost flat, whereas those of sites 3 to 6 exhibit  
 108 a subtle but clear feature at 2.7 μm. The presence of this feature in  
 109 the ratio spectra indicates that the OH feature is slightly stronger  
 110 and that the absorption peak is shifted toward a shorter wavelength  
 111 within the spectral resolution of NIRS3 for the ejecta-rich sites com-  
 112 pared with typical surface materials. Similar spectral differences  
 113 have not previously been confirmed in any other surface materi-  
 114 als on Ryugu, suggesting that these are intrinsic properties of the  
 115

116  
 117 **Fig. 1 | NIRS3 observations of the SCI crater region.** **a**, Context image  
 118 taken by the ONC-T camera. The dashed semi-circle represents the rim  
 119 of the SCI crater<sup>4</sup>. The arrows indicate the motion of NIRS3 footprints  
 120 during three descent operations. **b**, NIRS3 spectra averaged over regions  
 121 corresponding to the coloured boxes shown in **a**. The colour of each site  
 122 represents its surface characteristics: magenta, green and cyan are the  
 123 ejecta-free region, ejecta-rich region outside the crater and ejecta-rich  
 124 region inside the crater, respectively. Error bars are 1σ within the boxes.  
 125 Individual spectra of each site are shown in Extended Data Fig. 1. **c**, Ratios  
 126 of the normalized spectra shown in **b** to the ones of the surface standard  
 127 observed on the day before. The spectra are normalized and vertically  
 128 shifted for clarity. The dashed vertical lines at 2.72 μm denote the peak  
 129 wavelength of the OH absorption of the spectra in **b**.

subsurface material. Because the ejecta deposits have been found to  
 span the sampling site<sup>9</sup>, the samples to be returned by Hayabusa2  
 are expected to contain both surface and subsurface materials for  
 comparison in laboratory.

Previous laboratory studies have shown that the peak wavelength  
 of the OH absorption band varies with the Mg/Fe ratio of phyllo-



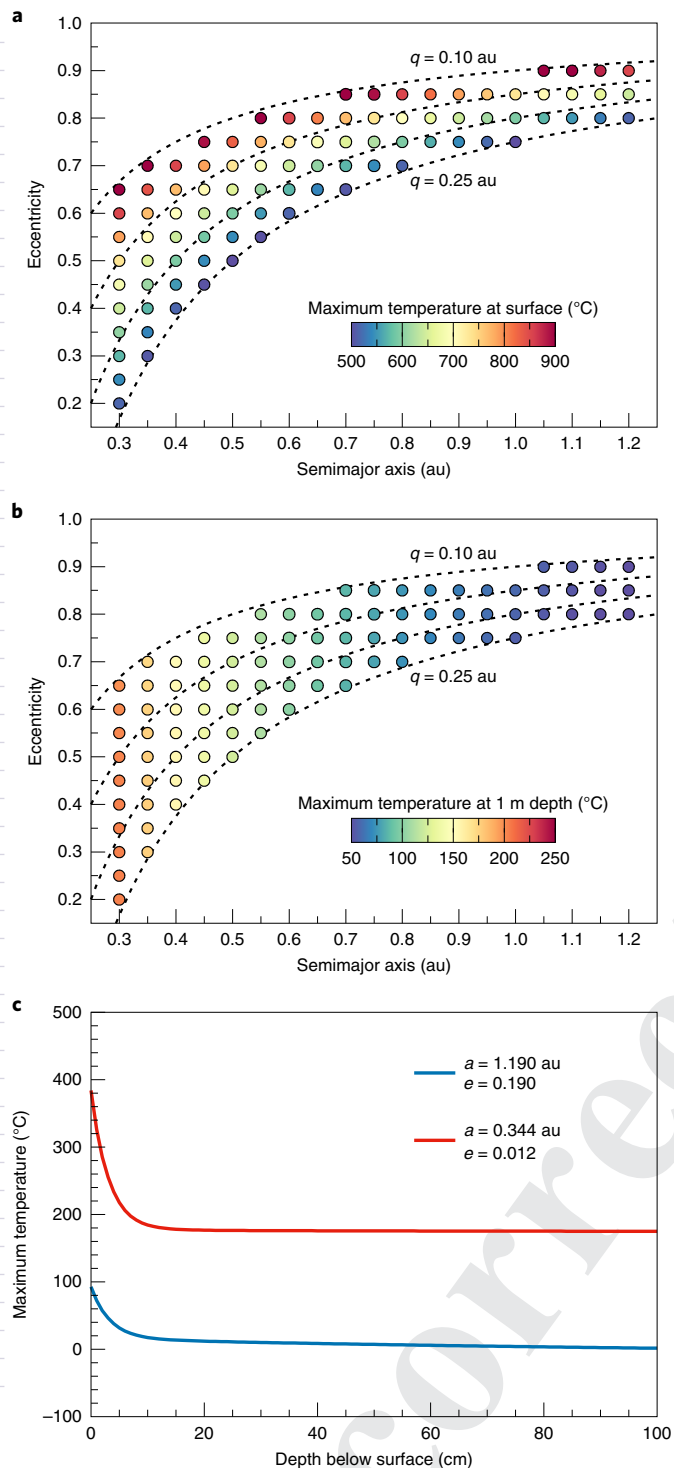


**Fig. 2 | Maximum surface and subsurface temperatures at the SCI crater region.** **a**, Maximum surface temperature for one revolution at a given Sun-approaching orbit. A grain density of  $2,420 \text{ kg m}^{-3}$ , a porosity of 41%, a thermal conductivity of  $0.16 \text{ W m}^{-1} \text{ K}^{-1}$ , and a temperature-dependent heat capacity<sup>37</sup> have been assumed. The dashed curves denote the perihelion distance  $q$  of 0.10, 0.15, 0.20 and 0.25 au. **b**, Same as **a** but for a depth of 1 m. **c**, Maximum temperature profile at the current orbit (blue) and the closest orbit to the Sun (red).

cate that the OH band position does not closely correlate with grain size and/or porosity<sup>12</sup>, thus it is unlikely that intrinsic physical attributes can explain the spectral differences between surface and subsurface materials on Ryugu. Indeed, there is currently no evidence in the Thermal Infrared Imager (TIR) data to indicate differences in grain size and/or porosity for the SCI crater region<sup>13</sup>. Alternatively, space weathering can be considered as a likely cause of the observed spectral differences. Solar wind ion irradiation, a primary source of space weathering, affects the surface at depths of tens to hundreds of nanometres and preferentially sputters the volatile and lighter Mg compared with Fe<sup>14,15</sup>. Recent laboratory experiments show that near-infrared spectra of irradiated phyllosilicates measured under vacuum conditions exhibit a similar shift in the OH band position as observed on Ryugu<sup>16</sup>. It is also possible that radiative heating may induce a change in the Mg/Fe ratio of phyllosilicates, but there is currently no available experimental data under relevant conditions to evaluate this possibility.

In spite of some differences from the surface, the overall spectral properties of the subsurface material on Ryugu still support a close similarity with thermally and/or shock metamorphosed carbonaceous chondrites. As previously discussed in ref. <sup>8</sup>, the material on Ryugu was likely aqueously altered to a greater extent than indicated by the current weak OH feature, and the aqueously altered material was then heated to high enough temperatures to induce loss of  $\text{H}_2\text{O}$  but only partial dehydroxylation. This process seems to have affected materials that are currently within the upper 1 m of Ryugu. This raises questions as to the source of the heating: thermal alteration due to radiogenic and/or impact heating on the original parent body<sup>17–19</sup>, or radiative heating during previous close encounters with the Sun<sup>20,21</sup>? The orbits of near-Earth asteroids evolve chaotically due to a combination of close encounters with the terrestrial planets and resonances with the giant planets<sup>22</sup>. A theoretical study shows the possibility that Ryugu's perihelion distance may have been as small as 0.1 au in the course of its history, resulting in surface temperatures as high as  $\sim 1,200$  °C (ref. <sup>20</sup>). This suggests that radiative heating might be able to easily explain the thermal alteration of Ryugu's surface, and a recent study suggests this form of heating has likely influenced the spectral properties of Ryugu at visible wavelengths<sup>21</sup>. However, these studies do not consider thermal effects at the excavation depth of the SCI crater, thus we examine the range of temperatures that the subsurface material could have experienced by using a thermophysical model (see Methods).

Figure 2a and b show the maximum temperatures achieved at the surface and at 1 m depth, respectively, for one orbital revolution. We find that the maximum temperature of the surface increases with decreasing perihelion distance, whereas temperatures at 1 m depth increase with decreasing semimajor axis. The surface temperature reaches values of 700 °C at a perihelion distance of 0.15 au, and laboratory spectra of the heated Ivuna CI chondrite sample exhibit the complete loss of OH features above this temperature (Fig. 3). The persistence of an OH feature on Ryugu suggests that it never approached the Sun at a distance less than 0.15 au. In addition, dynamical models of near-Earth asteroids indicate that there is no object having an orbit entirely inside that of Mercury's orbit<sup>23–25</sup>, and that their semimajor axis is never less than 0.344 au (ref. <sup>24</sup>). For that semimajor axis, the maximum temperature experienced at a depth of 1 m is estimated to be less than 200 °C (Fig. 2c). If impact gardening and mixing occur simultaneously with radiative heating, then materials that have experienced more heating might be able to exist in the subsurface. However, such mixing would act to homogenize the materials vertically and cannot explain the observed spectral differences between surface and subsurface materials. Thus, we can constrain the radiative heating of the material at the excavation depth of the SCI crater to below 200 °C.

Although it is difficult to estimate the exact temperature to which materials on Ryugu have been heated, the presence of a weak and

silicates in carbonaceous chondrites<sup>10,11</sup>. This would suggest that the subsurface material on Ryugu is more enriched in Mg–OH phyllosilicates relative to surface materials. Laboratory spectra also indi-

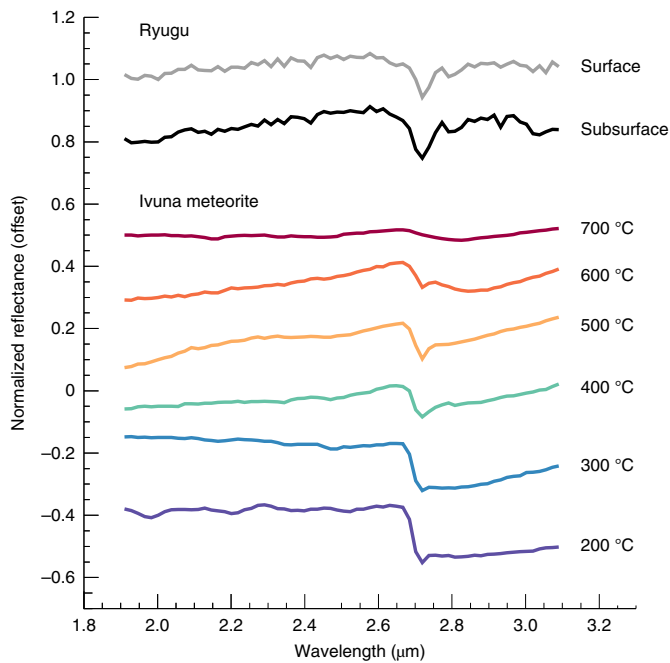


**Fig. 3 | Ryugu's surface and subsurface spectra compared with laboratory spectra of heated Ivuna meteorite sample.** The spectra of Ivuna meteorite taken from the Reflectance Experiment Laboratory (RELAB) database<sup>38</sup> are resampled with the same resolution as the Ryugu spectra. The spectra are normalized and vertically shifted for clarity.

narrow OH feature in Ryugu's spectra supports temperatures above 300 °C but below 700 °C, as demonstrated by the dehydration and partial dehydroxylation of Mg-rich phyllosilicates within this temperature range<sup>26</sup>. It is also possible that a weak OH feature occurs due to incomplete hydration reactions on the parent body, but the OH band position of 2.72 μm is more indicative of Ryugu's material having experienced a high degree of aqueous alteration<sup>27</sup>. We thus consider that the primary process of thermal alteration for material on Ryugu is more consistent with radiogenic and impact heating on the parent body from which it formed rather than radiative heating after re-accretion and formation. Extended Data Figs. 1–4.

## Methods

**Location of the NIRS3 footprints.** The spacecraft trajectories for observations of the SCI crater region have not been well determined due to frequent delta-v manoeuvres. Therefore, we identified the location of NIRS3 footprints using the continuous series of images acquired by the ONC-T camera during the SCI crater characterization activities. The boresight of NIRS3 is co-registered with the ONC-T field of view and the pixels of the ONC-T image corresponding to the NIRS3 footprint have been precisely determined<sup>28</sup>. To derive the footprints shown in Fig. 1a, we used 18 images taken from 02:36:15 to 02:40:39 on 16 May, 18 images taken from 02:35:44 to 02:40:07 on 30 May, and 12 images taken from 02:00:18 to 02:16:59 on 13 June.

**Analysis of the NIRS3 spectra.** Extended Data Fig. 2 shows the details of the NIRS3 spectra that we used for the analysis of the SCI crater region. The spectra of sites 3 and 4 and sites 5 and 6 were obtained under 9 °C and 10 °C higher detector temperatures, respectively, than the nominal value due to thermal flux from the surface of Ryugu. Because the responsivity of the detector changes with its temperature, we corrected that effect using additional calibration data obtained under the same temperature conditions. With the exception of this temperature correction the data processing is the same as previously published<sup>8</sup>.

To evaluate spectral differences between the surface and subsurface materials, we compared the spectra of the SCI crater region with those of regions not contaminated by the crater ejecta. Extended Data Fig. 3 shows the details of the NIRS3 spectra of regions that we chose as the surface standard. As shown in Extended Data Fig. 4, it has been found that a small residual of thermal correction appears between spectra of regions with different surface temperatures. To avoid such an artefact, we chose a region having a similar surface temperature to the SCI

crater region for the surface standard. Small variations in spectral slope among the spectra shown in Fig. 1c may be due to the thermal residual.

**Thermophysical modelling.** To investigate the effects of radiative heating on the SCI crater region, we set up a thermophysical model<sup>29</sup> that computes surface and subsurface temperatures on Ryugu with a Sun-approaching orbit. Taking into account the location of the SCI crater<sup>1</sup> and Ryugu's obliquity<sup>30</sup>, we assume a single facet on the equator of a spherical object having the spin axis perpendicular to its orbital plane. Because the SCI crater is located at the equatorial region, even if Ryugu's past obliquity was different, the maximum temperature would not exceed that of the current perpendicular spin case considered here. The facet temperature  $T$  as a function of time  $t$  and depth  $z$  is determined by numerically solving the one-dimensional heat conduction equation:

$$\rho(1 - \phi)c \frac{\partial T}{\partial t} = \kappa \frac{\partial^2 T}{\partial z^2} \quad (1)$$

where  $\rho$  is the grain density,  $\phi$  is the porosity,  $c$  is the specific heat capacity and  $\kappa$  is the thermal conductivity. Because Ryugu's surface is covered by decimetre- to metre-sized rocks without a fine-grained component<sup>31</sup>, we used the parameter values derived for a boulder on Ryugu from in situ measurements by the MASCOT lander<sup>32</sup>:  $\rho = 2,420 \text{ kg m}^{-3}$ ,  $\phi = 41\%$ ,  $\kappa = 0.16 \text{ W m}^{-1} \text{ K}^{-1}$  and a temperature-dependent heat capacity<sup>33,34</sup>. These are consistent with remote sensing measurements<sup>33,34</sup>.

The boundary condition at the surface is given by

$$\kappa \left( \frac{\partial T}{\partial z} \right)_{z=0} = \varepsilon \sigma T_{z=0}^4 - \frac{(1-A)S_{\odot}}{r^2} \max(0, \cos \theta) \quad (2)$$

where  $\varepsilon$  is the emissivity,  $\sigma$  is the Stefan–Boltzmann constant,  $A$  is the bond albedo,  $S_{\odot}$  is the solar constant at 1 au,  $r$  is the heliocentric distance in au, and  $\theta$  is the angle between the surface normal and the solar vector. The position of Ryugu with respect to the Sun at a given time is computed using the Kepler's equation solution<sup>35</sup>. We used a bond albedo of 0.0146 and an emissivity of 1.0 (ref. <sup>32</sup>), and assumed a constant rotational period of 7.6326 h (ref. <sup>30</sup>).

To ensure a sufficient depth for the seasonal temperature variations, we assumed an adiabatic boundary condition at 5 m depth:

$$\left( \frac{dT}{dz} \right)_{z=5 \text{ m}} = 0 \quad (3)$$

The current seasonal thermal skin depth of Ryugu is  $l_s = \sqrt{\kappa P_{\text{orb}} / 2\pi\rho(1 - \phi)c} \approx 1.1 \text{ m}$ , where  $P_{\text{orb}}$  is the orbital period, and it decreases with decreasing semimajor axis. We ran the model with a time step of 15 s and a depth step of 0.01 m. After 10 years integration, the results converged to temperature deviations of less than 1 K.

In the model, we used an emissivity of 1.0 as the nominal value considering the results of MASCOT<sup>32</sup>, but even in case of an emissivity of 0.9, the maximum temperatures of the surface and subsurface increase by only 15 K. In addition, we have also confirmed that the variation of maximum temperatures by the bond albedo uncertainty<sup>36</sup> is within 1 K.

## Data availability

The data that support the plots within this paper and other findings of this study are available from the corresponding author upon reasonable request. The raw and calibrated NIRS3 data will be made available through the JAXA Data Archives and Transmission System (DARTS) website (<https://darts.isas.jaxa.jp/planet/project/hayabusa2/>).

Received: 21 May 2020; Accepted: 10 November 2020;

## References

- Nakamura, T. Post-hydration thermal metamorphism of carbonaceous chondrites. *J. Miner. Petrol. Sci.* **100**, 260–272 (2005).
- Marchi, S., Delbo, M., Morbidelli, A., Paolicchi, P. & Lazzarin, M. Heating of near-Earth objects and meteoroids due to close approaches to the Sun. *Mon. Not. R. Astron. Soc.* **400**, 147–153 (2009).
- Chaumard, N., Devouard, B., Delbo, M., Provost, A. & Zanda, B. Radiative heating of carbonaceous near-Earth objects as a cause of thermal metamorphism for CK chondrites. *Icarus* **220**, 65–73 (2012).
- Arakawa, M. et al. An artificial impact on the asteroid 162173 Ryugu formed a crater in the gravity-dominated regime. *Science* **368**, 67–71 (2020).
- Saiki, T. et al. Hayabusa2's kinetic impact experiment: operational planning and results. *Acta Astronaut.* **175**, 362–374 (2020).
- Brunetto, R., Loeffler, M. J., Nesvorný, D., Sasaki, S. & Strazzulla, G. in *Asteroids IV* (eds Michel, P. et al.) 597–616 (University of Arizona Press, 2015).
- Iwata, T. et al. NIRS3: the near-infrared spectrometer on Hayabusa2. *Space Sci. Rev.* **208**, 317–337 (2017).

- 223 8. Kitazato, K. et al. The surface composition of asteroid 162173 Ryugu from  
 224 Hayabusa2 near-infrared spectroscopy. *Science* **364**, 272–275 (2019).  
 225 9. Tsuda, Y. et al. Hayabusa2 mission status: landing, roving and cratering on  
 226 asteroid Ryugu. *Acta Astronaut.* **171**, 42–54 (2020).  
 227 10. Beck, P. et al. Hydrous mineralogy of CM and CI chondrites from infrared  
 228 spectroscopy and their relationship with low albedo asteroids. *Geochim.*  
 229 *Cosmo. Acta* **75**, 4881–4892 (2010).  
 230 11. Takir, D. et al. Nature and degree of aqueous alteration in CM and CI  
 231 carbonaceous chondrites. *Meteorit. Planet. Sci.* **48**, 1618–1637 (2013).  
 232 12. Potin, S., Beck, P., Schmitt, B. & Moynier, F. Some things special about NEAs:  
 233 geometric and environmental effects on the optical signatures of hydration.  
 234 *Icarus* **333**, 415–428 (2019).  
 235 13. Sakatani, N. et al. Thermophysical property of the artificial impact crater on  
 236 asteroid Ryugu. In *51st Lunar Planet. Sci. Conf.* Abstract no. 2326 (2020).  
 237 14. Lantz, C. et al. Ion irradiation of carbonaceous chondrites: a new view of  
 238 space weathering on primitive asteroids. *Icarus* **285**, 43–57 (2017).  
 239 15. Brunetto, R. et al. Hyperspectral FTIR imaging of irradiated carbonaceous  
 240 meteorites. *Planet. Space Sci.* **158**, 38–45 (2018).  
 241 16. Rubino, S. et al. Space weathering affects the remote near-IR identification of  
 242 phyllosilicates. *Planet. Sci. J.* (in the press).  
 243 17. Sugita, S. et al. The geomorphology, color, and thermal properties  
 244 of Ryugu: implications for parent-body processes. *Science* **364**, eaaw0422  
 245 (2019).  
 246 18. Michel, P. et al. Collisional formation of top-shaped asteroids and implications  
 247 for the origins of Ryugu and Bennu. *Nat. Commun.* **11**, 2655 (2020).  
 248 19. Amsellem, E., Moynier, F., Mahan, B. & Beck, P. Timing of thermal  
 249 metamorphism in CM chondrites: implications of Ryugu and Bennu future  
 250 sample return. *Icarus* **339**, 113593 (2020).  
 251 20. Michel, P. & Delbo, M. Orbital and thermal evolutions of four potential  
 252 targets for a sample return space mission to a primitive near-Earth asteroid.  
 253 *Icarus* **209**, 520–534 (2010).  
 254 21. Morota, T. et al. Sample collection from asteroid (162173) Ryugu  
 255 by Hayabusa2: implications for surface evolution. *Science* **368**,  
 256 654–659 (2020).  
 257 22. Morbidelli, A., Bottke, W. F., Froeschlé, C. & Michel, P. in *Asteroids III* (eds  
 258 Bottke, W. F. et al.) 409–422 (University of Arizona Press, 2002).  
 259 23. Bottke, W. F. et al. Debiased orbital and absolute magnitude distribution of  
 260 the near-Earth objects. *Icarus* **156**, 399–433 (2002).  
 261 24. Greenstreet, S., Ngo, H. & Gladman, B. The orbital distribution of near-Earth  
 262 objects inside Earth's orbit. *Icarus* **217**, 355–366 (2012).  
 263 25. Granvik, M. et al. Debiased orbit and absolute-magnitude distributions for  
 264 near-Earth objects. *Icarus* **312**, 181–207 (2018).  
 265 26. King, A. J., Solomon, J. R., Schofield, P. F. & Russell, S. S. Characterising the  
 266 CI and CI-like carbonaceous chondrites using thermogravimetric analysis  
 267 and infrared spectroscopy. *Earth Planet. Space* **67**, 198 (2015).  
 268 27. Bates, H. C. et al. Linking mineralogy and spectroscopy of highly aqueously  
 269 altered CM and CI carbonaceous chondrites in preparation for primitive  
 270 asteroid sample return. *Meteorit. Planet. Sci.* **55**, 77–101 (2020).  
 271 28. Tatsumi, E. et al. Updated inflight calibration of Hayabusa2's optical  
 272 navigation camera (ONC) for scientific observations during the cruise phase.  
 273 *Icarus* **325**, 153–195 (2019).  
 274 29. Spencer, J. R. et al. Systematic biases in radiometric diameter determinations.  
 275 *Icarus* **78**, 337–354 (1989).  
 276 30. Watanabe, S. et al. Hayabusa2 arrives at the carbonaceous asteroid 162173  
 277 Ryugu—a spinning top-shaped rubble pile. *Science* **364**, 268–272 (2019).  
 278 31. Jaumann, R. et al. Images from the surface of asteroid Ryugu show rocks  
 279 similar to carbonaceous chondrite meteorites. *Science* **365**, 817–820 (2019).  
 280 32. Grott, M. et al. Low thermal conductivity boulder with high porosity  
 281 identified on C-type asteroid (162173) Ryugu. *Nat. Astron.* **3**, 971–976 (2019).  
 282 33. Okada, T. et al. Highly porous nature of a primitive asteroid revealed by  
 283 thermal imaging. *Nature* **579**, 518–522 (2020).  
 284 34. Shimaki, Y. et al. Thermophysical properties of the surface of asteroid 162173  
 285 Ryugu: infrared observations and thermal inertia mapping. *Icarus* (under  
 286 review).  
 287 35. Murray, C. D. & Dermott, S. F. *Solar System Dynamics* (Cambridge Univ.  
 288 Press, 1999).  
 36. Ishiguro, M. et al. Optical properties of (162173) 1999 JU3: in preparation for  
 the JAXA Hayabusa 2 sample return mission. *Astrophys. J.* **792**, 74 (2014).  
 37. Wada, K. et al. Asteroid Ryugu before the Hayabusa2 encounter. *Prog. Earth  
 Planet. Sci.* **5**, 82 (2018).  
 38. Hiroi, T. et al. Reflectance spectra (UV–3µm) of heated Ivuna (CI) meteorite  
 and newly identified thermally metamorphosed CM chondrites. In *27th  
 Lunar Planet. Sci. Conf.* Abstract no. 551 (1996).

### Acknowledgements

The Hayabusa2 NIRS3 was funded by JAXA and built by Meisei Electric, Genesis and Hamamatsu Photonics. We thank H. Murao, Y. Sakata, A. Ikeda and K. Taguchi for their efforts in the development of NIRS3. We acknowledge the support from JAXA, CNES and ASI. D.L.D. and D.T. were supported by NASA's Hayabusa2 Participating Scientist Program (NNX17AL02G, NNX16AL34G). D.L.D. was supported by the SSERVI16 Cooperative Agreement (NNH16ZDA001N). A part of this study was supported by the JSPS Grant-in-Aid for Scientific Research (16H04044, 17H06459, 17K05639) and the JSPS Core-to-Core Program (17H01175).

### Author contributions

K.K. led the study, performed the data analysis and thermophysical modeling and wrote the manuscript. R.E.M. contributed to the interpretation of the results and assisted in the writing. T.I. led the development of NIRS3. M.A., M.O., S.M., M.M., L.R., Y.N., T.K. and T.A. contributed to the development and operation of NIRS3. L.R., C.P., D.L.D., E.P. and A.G. contributed to the data analysis. Y.T., T.N., T.H., M.M., L.R., M.A.B., R.B., C.P., F.P., D.L.D., F.V., D.T., E.P. and A.G. participated in the interpretation of the results. All authors participated in science data acquisition, mission planning, mission operations, or project management, and/or contributed to discussion of the results. The entire Hayabusa2 project team made this mission possible.

### Competing interests

The authors declare no competing interests.

### Additional information

**Extended data** is available for this paper at <https://doi.org/10.1038/s41550-020-01271-2>.

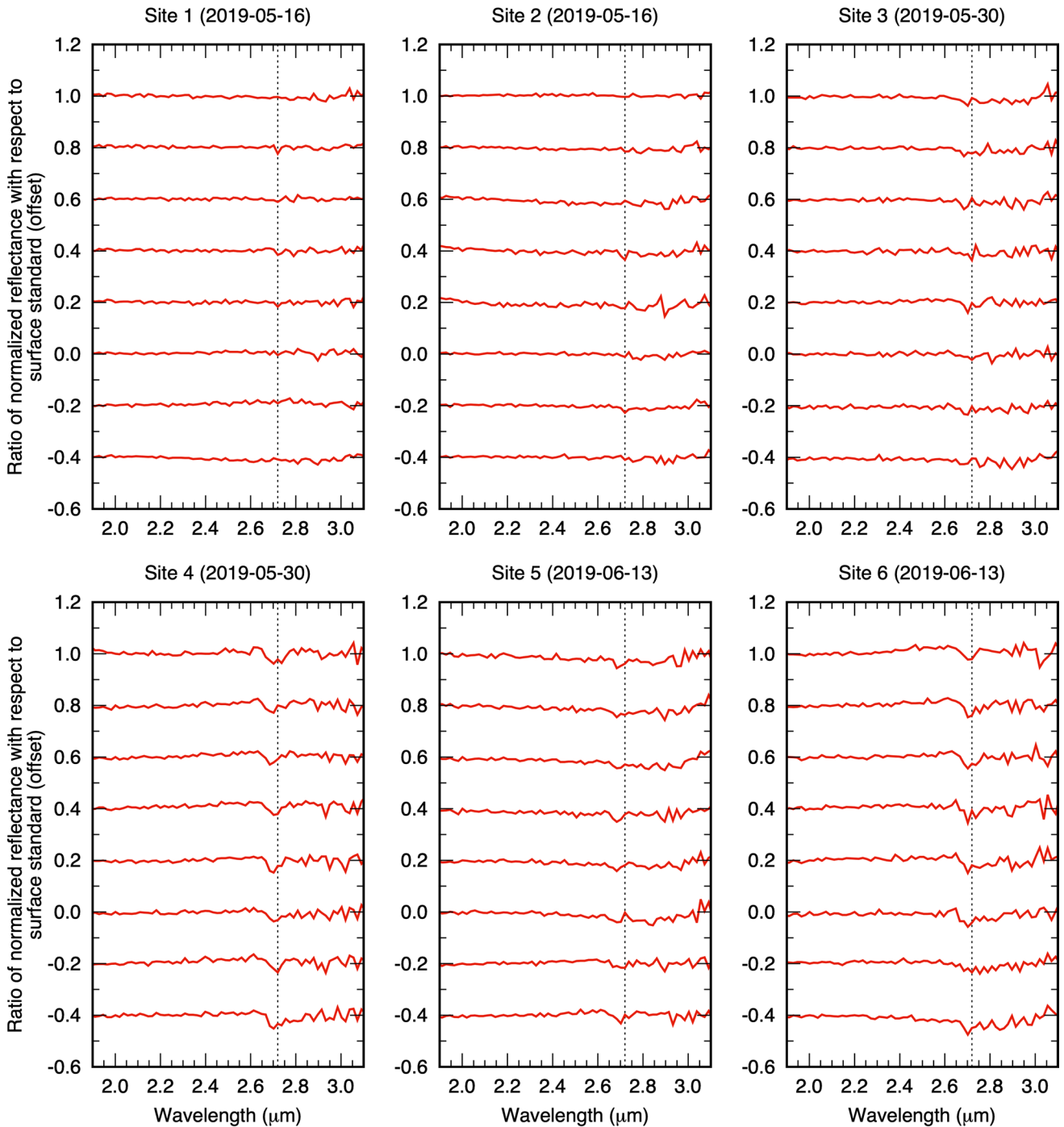
**Correspondence and requests for materials** should be addressed to K.K.

**Peer review information** *Nature Astronomy* thanks Pierre Beck, Benoit Carry and Ellen Howell for their contribution to the peer review of this work.

**Reprints and permissions information** is available at [www.nature.com/reprints](http://www.nature.com/reprints).

**Publisher's note** Springer Nature remains neutral with regard to jurisdictional claims in published maps and institutional affiliations.

© The Author(s), under exclusive licence to Springer Nature Limited 2020



**Extended Data Fig. 1 | Individual spectra from each site used to derive the average spectra of the SCI crater region.** The spectra are divided by the surface standard spectrum of the day before and vertically shifted for clarity.

289  
290  
291  
292  
293  
294  
295  
296  
297  
298  
299  
300  
301  
302  
303  
304  
305  
306  
307  
308  
309  
310  
311  
312  
313  
314  
315  
316  
317  
318  
319  
320  
321  
322  
323  
324  
325  
326  
327  
328  
329  
330  
331  
332  
333  
334  
335  
336  
337  
338  
339  
340  
341  
342  
343  
344  
345  
346  
347  
348  
349  
350  
351  
352  
353  
354

A

B

Site #	Observation date and time (UTC)	# of spectra	Solar distance (au)	Phase angle (°)	LIDAR range (m)	Surface temp. (°C)
1	2019-05-16 02:36:21 – 02:37:46	8	1.25	31.1	–	35 <sup>+9</sup> <sub>–9</sub>
2	02:38:50 – 02:40:16	8	1.25	31.1	–	23 <sup>+16</sup> <sub>–15</sub>
3	2019-05-30 02:35:50 – 02:37:16	8	1.21	33.7	252 – 277	41 <sup>+7</sup> <sub>–8</sub>
4	02:38:30 – 02:39:56	8	1.21	33.7	298 – 325	50 <sup>+7</sup> <sub>–9</sub>
5	2019-06-13 02:00:17 – 02:01:43	8	1.17	35.7	82 – 107	41 <sup>+17</sup> <sub>–12</sub>
6	02:02:26 – 02:03:51	8	1.17	35.7	119 – 145	42 <sup>+20</sup> <sub>–13</sub>

**Extended Data Fig. 2 |** Details of observations of the SCI crater region. Add caption.

Observation date and time (UTC)	# of spectra	Longitude (°)	Latitude (°)	LIDAR range (km)	Surface temp. (°C)
2019-05-15 10:22:09 – 10:44:56	128	321 – 340	4 – 7	8.5 – 9.0	32 <sup>+7</sup> <sub>-11</sub>
2019-05-29 06:58:34 – 07:21:21	128	112 – 136	-33 – -30	13.1 – 13.7	40 <sup>+5</sup> <sub>-9</sub>
2019-06-12 02:46:54 – 03:09:41	128	314 – 327	-44 – -29	18.5 – 19.1	44 <sup>+2</sup> <sub>-1</sub>

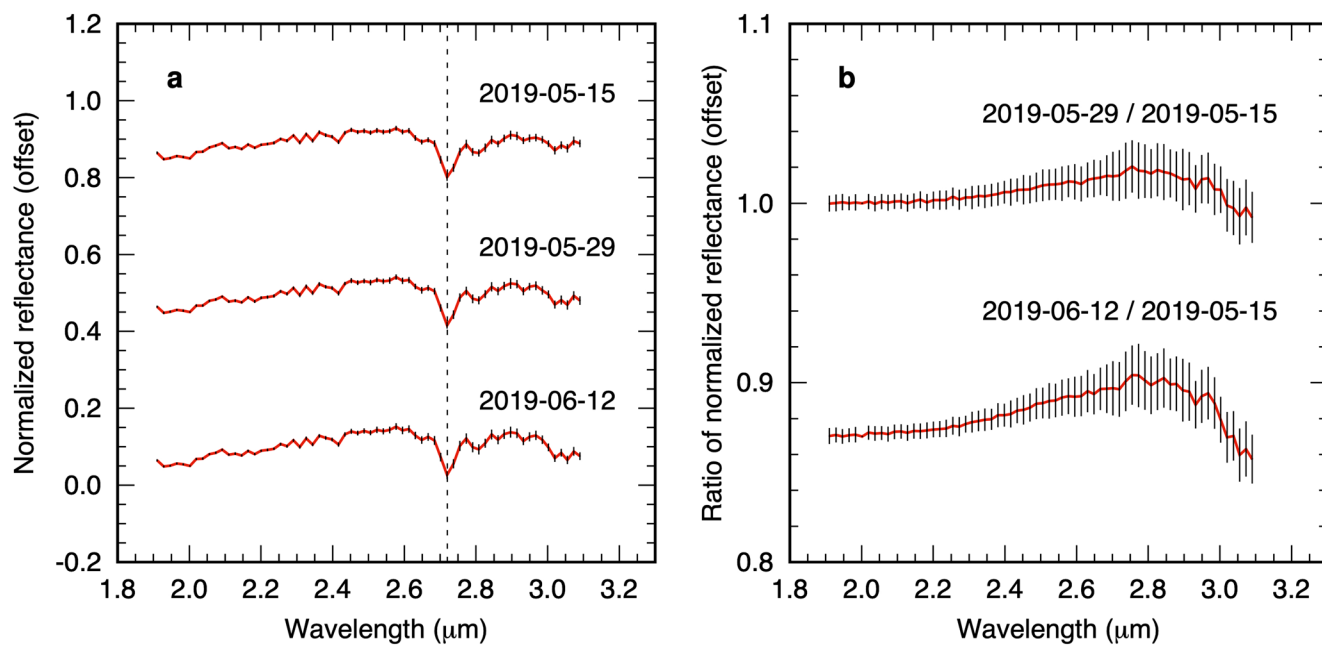
**Extended Data Fig. 3 |** Details of observations of the surface standard. Add caption.

Uncorrected proofs

421  
422  
423  
424  
425  
426  
427  
428  
429  
430  
431  
432  
433  
434  
435  
436  
437  
438  
439  
440  
441  
442  
443  
444  
445  
446  
447  
448  
449  
450  
451  
452  
453  
454  
455  
456  
457  
458  
459  
460  
461  
462  
463  
464  
465  
466  
467  
468  
469  
470  
471  
472  
473  
474  
475  
476  
477  
478  
479  
480  
481  
482  
483  
484  
485  
486

A

B



**Extended Data Fig. 4 | NIR3 spectra of the surface standard.** **a**, Spectra averaged over regions having the similar surface temperature to the SCI crater region. The details of these spectra are listed in Extended Data Fig. 3. **b**, Ratios between the normalized spectra shown in **a**. The non-flat shape of the ratio-spectra indicates the residual of thermal correction. The spectra are normalized and vertically shifted for clarity. Note that the vertical scale of **b** is much larger than that of **a** to show the curvature and uncertainties of the ratio-spectra.

# QUERY FORM

<b>Nature Astronomy</b>	
<b>Manuscript ID</b>	[Art. Id: 1271]
<b>Author</b>	<b>K. Kitazato</b>

**AUTHOR:**

The following queries have arisen during the editing of your manuscript. Please answer by making the requisite corrections directly in the e-proofing tool rather than marking them up on the PDF. This will ensure that your corrections are incorporated accurately and that your paper is published as quickly as possible.

<b>Query No.</b>	<b>Nature of Query</b>
Q1:	In the sentence beginning 'However, the lack of direct measurements', what exactly is 'it' referring to? Can you reword to clarify please.
Q2:	Please check your article carefully, coordinate with any co-authors and enter all final edits clearly in the eproof, remembering to save frequently. Once corrections are submitted, we cannot routinely make further changes to the article.
Q3:	Note that the eproof should be amended in only one browser window at any one time; otherwise changes will be overwritten.
Q4:	Author surnames have been highlighted. Please check these carefully and adjust if the first name or surname is marked up incorrectly. Note that changes here will affect indexing of your article in public repositories such as PubMed. Also, carefully check the spelling and numbering of all author names and affiliations, and the corresponding email address(es).
Q5:	If applicable, please ensure that any accession codes and datasets whose DOIs or other identifiers are mentioned in the paper are scheduled for public release as soon as possible, we recommend within a few days of submitting your proof, and update the database record with publication details from this article once available.
Q6:	Have edits to the sentence beginning 'In addition, dynamical models of' retained your intended meaning?
Q7:	For Fig. 2c, please define a and e.
Q8:	Please cite Extended Data Figs. 1-4 in the main text and delete the temporary citations from here.
Q9:	In the sentence beginning 'The boresight of NIRS3 is co-registered', should 'ONCT-T' be 'ONC-T'?
Q10:	Edits to the sentence beginning 'The spectra of sites' OK?
Q11:	In the sentence beginning 'Because Ryugu's surface is covered', please define 'MASCOT'.
Q12:	In the author contributions section, can you please specify who the following initials belong to: (1) please change 'M.A.' to 'M. Abe' or 'M. Arakawa'; (2) change 'M.O.' to 'M. Ohtake' or 'M. Ozaki'; (3) change 'T.K.' to 'T. Kadono' or 'T. Kouyama'; (4) change 'Y.T.' to 'Y. Takagi', 'Y. Takei' or 'Y. Tsuda'; (5) for initials 'T.A.', there are two instances of 'T. Arai' in the author list, can you please differentiate between the two by either adding a middle initial or spelling out the first name, and update here accordingly.
Q13:	Please provide a caption for Extended Data Fig. 3.

